Journal Homepage: -www.journalijar.com

INTERNATIONAL JOURNAL OF ADVANCED RESEARCH (IJAR)

Article DOI:10.21474/IJAR01/10293
DOI URL: http://dx.doi.org/10.21474/IJAR01/10293

ISSN NO. 2320-5407

RESEARCH ARTICLE

CONDITIONSTO REALIZE HEXAROTOR STABLE FLIGHTS TO AVOID A CRASH UNDER COMPLETE PROPELLOR MOTOR FAILURES

Kaito Isogai and Hideaki Okazaki
Graduate School of Electrical and Information Engineering, Shonan Institute of Technology, 1-1-25 Tsujido Nishikaigan, Fujisawa 251-8511, Japan.

Manuscript Info

Manuscript History
Received: 23 November 2019
Final Accepted: 25 December 2019
Published: January 2020

Key words:-
Hexarotor, Motor Failure Problem, Stable Flights To Avoid a Crash

Abstract

In this paper, in the case of complete propeller motor failures, a feedback-loop control for a multirotor to avoid a crash when some motors fail and stop, is presented, and verified by simulation results. First, the modeling foundation for a multirotor, and the flight states are summarized. Secondly, theorems of the stabilizability of the flight states for avoiding a crash, by nonlinear dynamic state equations with state variable feedbacks are provided, andalso verified by simulations. In conclusion, the principal results are summarized, and the future research is described.

Introduction:-

Multirotors using fixed motors for flight, have been widely used in many applications, such as agriculture, surveillance and search, entertainment, photography, and rescue missions. However, there are the risks resulting in injury or deaths and damages if multirotors crash. Therefore, multirotor flight crash avoidances in the case of complete motor failures have been studied [2], [4]-[7], [11], [12], [14]-[16], [18]-[20]. However, feedback-loop controls to avoid a crash for both configurations, have been seldom studied. Especially the establishment of the hexarotor feedback-loop controls to avoid a crash, is very important under general Euler angle rotational motions.On the other hand, the authors obtained the maneuver and flight states for multirotors (a quadrotor, a hexarotor, or an octorotor) with standard symmetrical configurations, based on both of the general Euler angle rotational motion and the translational motion of the state equations. They provided definitions of the operating points and equilibrium points of multirotors, and definitions of multirotor motor speed control signal vectors. Further they provided “add-on to underdetermined system equations” method of directly providing motor speed control signals for hexarotor or octorotor flights to avoid crashes (an open-loop control) when some motors fail and stop, and illustrated typical examples of hexarotor or octorotor flight states to avoid crashes obtained by the method [12]. Hence in this paper, to solve the problem to avoid a crash for the hexarotor in the case of complete failures, we expand on “add-on to underdetermined system equations” method based on [11], [12], [16], [18], and build a feedback-loop control to avoid a crash such that the hexarotor flight states to avoid crashes are stably realized when some motors fail and stop. First, we summarize the modeling foundation for a hexarotor, the maneuvers, and the flight states. Secondly, we provide theorems of the stabilizability of the flight states for avoiding a crash and stabilizing such flight states by nonlinear dynamic state equations with state variable feedbacks. Thirdly, we verify the theorems by simulations of the hexarotor stable flights to avoid a crash in the case of complete propeller motor failures. In Conclusion, we summarize the principal results and describe future research.

Corresponding Author:- Kaito Isogai
Address**:-** Graduate School of Electrical and Information Engineering, Shonan Institute of Technology, 1-1-25 TsujidoNishikaigan, Fujisawa 251-8511, Japan.

Mathematical Description of a Multirotor:-

In this section, we summarize the mathematical foundation for describing the motion of a multirotor as a rigid body, and multirotor body frame configurations. We also describe dynamical Euler angle state equations of rotations, dynamical system state equations of translations, and the maneuvers and flight states (or operating points) based on [12].

Rigid-body dynamics:-

Table 1:- Describes the symbols for the motion of a multirotor as a rigid body based [1].

Symbol	Description
$\mathbb{R}^3$	Three-dimensional real vector space
$t \in \mathbb{R}$	Time
w: $\boldsymbol{O} + span\{\boldsymbol{e}_1, \boldsymbol{e}_2, \boldsymbol{e}_3\}$.[15]	Basis vectors of a right-handed Cartesian stationary coordinate system at the origin $\boldsymbol{O}$ (Fig. 1)
W: $\boldsymbol{O}_c + span\{\boldsymbol{E}_1, \boldsymbol{E}_2, \boldsymbol{E}_3\}$ or ($\boldsymbol{O}_c + span\{\boldsymbol{e}_1, \boldsymbol{e}_2, \boldsymbol{e}_3\}$).[15]	Basis vectors of a right-handed moving (or local) coordinate system connected to the body at the center of mass $\boldsymbol{O}_c$
$\boldsymbol{B}$	Linear operator, $\boldsymbol{B}$: $W \to w$
$\boldsymbol{q} \in w$	Radius vector of a point moving relative to the stationary system
$\boldsymbol{Q}(t)$	Radius vector of the point relative to the moving system such that $\boldsymbol{q} = \boldsymbol{r} + \boldsymbol{BQ}$
$\dot{\boldsymbol{q}}$	Absolute velocity such that $\dot{\boldsymbol{q}} = \dot{\boldsymbol{r}} + \dot{\boldsymbol{B}}\boldsymbol{Q} + \boldsymbol{B}\dot{\boldsymbol{Q}}$, where an overdotrepresents time differentiation
$\boldsymbol{r}$	Radius vector of the moving coordinate system relative to the stationary coordinate system
$\dot{\boldsymbol{r}}$	Velocity of motion of the moving coordinate system
$\boldsymbol{\Omega} \in W$	Vector of angular velocity in multirotors such that $\boldsymbol{\Omega} = \boldsymbol{B}^{\mathrm{T}}\boldsymbol{\omega}$
$\boldsymbol{\omega} \in w$	Instantaneous angular velocity
$\hat{I}$ ($I_{11} \neq 0, I_{22} \neq 0, I_{33} \neq 0, I_{ij} = 0,$ for $i \neq j$)	Moment of inertia for multirotors

Table 1:- Mathematical description for the motion of a multirotor as a rigid body [12].

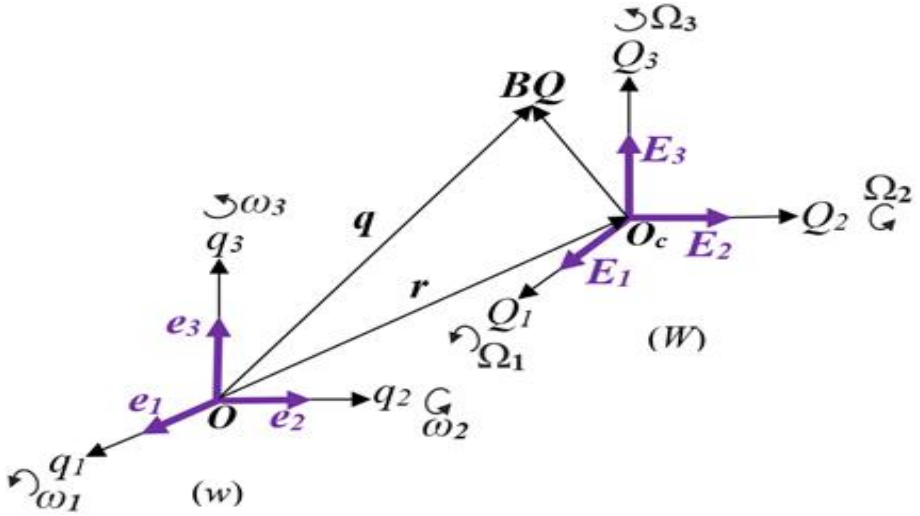

Fig. 1:- Radius vector of a point with respect to stationary (w) and moving (W) coordinate systems[12].

In addition, linear operator$\boldsymbol{B}$is also described by a matrix form:-

$$\boldsymbol{B} = \begin{Bmatrix} \cos\psi\cos\theta & \cos\psi\sin\theta\sin\phi - \sin\psi\cos\phi & \cos\psi\sin\theta\cos\phi + \sin\psi\sin\phi \\ \sin\psi\cos\theta & \sin\psi\sin\theta\sin\phi + \cos\psi\cos\phi & \sin\psi\sin\theta\cos\phi - \cos\psi\sin\phi \\ -\sin\theta & \cos\theta\sin\phi & \cos\theta\cos\phi \end{Bmatrix}. \qquad (2.1)$$

The angles $\psi, \theta,$ and$\phi$are Tait–Bryan angles and are examples of the Euler angles [8],[13].

Description of multirotor body frame configuration:-

We assume that all rotors are the same, distributed evenly, and coplanar, and the distance from each rotor to the geometric center of the multirotor ℓis equal [6]. Eachmultirotor has a standard symmetrical configuration with a clockwise-rotating rotor adjacent to a counterclockwise-rotating rotor as shown in Figs. 2–4.

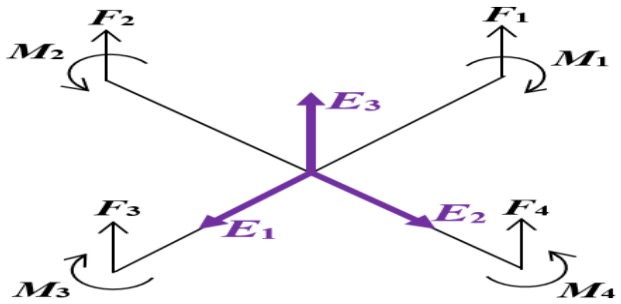

Fig. 2:- Quadrotor with standard configuration.

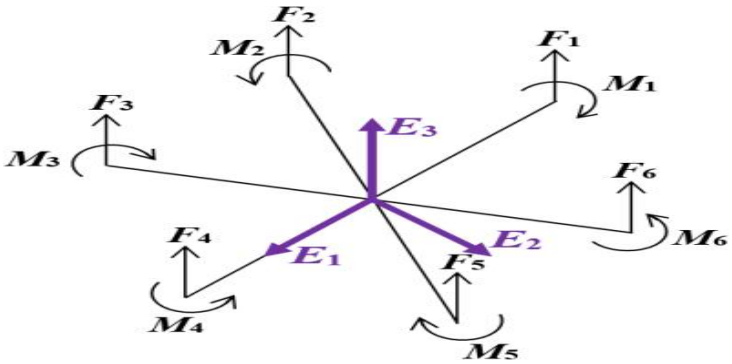

Fig. 3:- Hexarotor with standard configuration

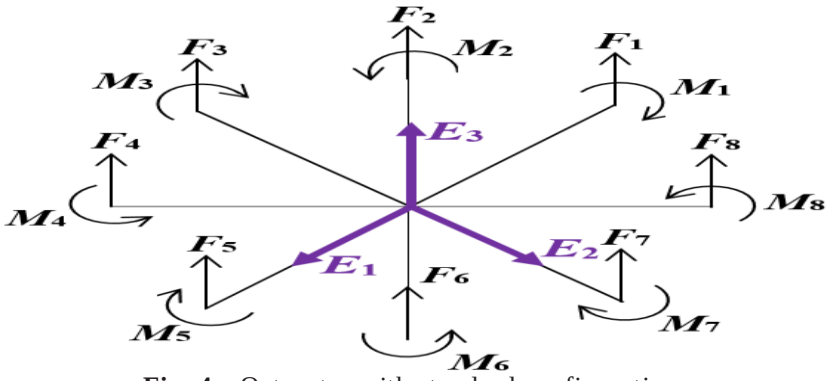

Fig. 4:- Octorotor with standard configuration.

$F_i(i = 1, 2, \dots, 2p, p = 2, 3, 4)$and $M_i(i = 1, 2, \dots, 2p, p = 2, 3, 4)$in Figs.2–4represent vertical forces and moments, respectively.Each motor of a multirotor has an angular speed ω_{Mi} and produces a vertical force $F_i$satisfying

$$F_i = k_{Fi}\omega_{Mi}^2, \quad i = 1, 2, \dots, 2p, p = 2, 3, 4. \qquad (2.2)$$

Each motor also produces the moment

$$M_i = k_{Mi}\omega_{Mi}^2, \quad i = 1, 2, \dots, 2p, p = 2, 3, 4. \qquad (2.3)$$

In practice, simple lumped parameter models are applied such that $k_F > 0$ and $k_M > 0$ are constants that can be easily determined from static thrust tests. For quadrotors ($p = 2$), hexarotors ($p = 3$), and octorotors ($p = 4$) that have standard symmetrical configurations, we define the moments of $\boldsymbol{S}_{\mathrm{rot}2p}\boldsymbol{u}_{2p}$ and the translational forces of $\boldsymbol{S}_{\mathrm{tra}2p}\boldsymbol{u}_{2p}, p = 2, 3, 4$, as follows.

For quadrotors($p = 2$),

$$\boldsymbol{S}_{\text{rot4}} = \begin{pmatrix} 0 & -\ell \cdot k_{F2} & 0 & \ell \cdot k_{F4} \\ \ell \cdot k_{F1} & 0 & -\ell \cdot k_{F3} & 0 \\ -k_{M1} & k_{M2} & -k_{M3} & k_{M4} \end{pmatrix}, \tag{2.4}$$

$$\boldsymbol{u}_4 = \sum_{i=1}^{4} \omega_{Mi}^2 \boldsymbol{\varepsilon}_{Mi}. \tag{2.5}$$

For hexarotors($p = 3$),

$$\boldsymbol{S}_{\text{rot6}} = \begin{pmatrix} 0 & -\frac{\sqrt{3}}{2}\ell \cdot k_{F2} & -\frac{\sqrt{3}}{2}\ell \cdot k_{F3} & 0 & \frac{\sqrt{3}}{2}\ell \cdot k_{F5} & \frac{\sqrt{3}}{2}\ell \cdot k_{F6} \\ \ell \cdot k_{F1} & 0.5\ell \cdot k_{F2} & -0.5\ell \cdot k_{F3} & -\ell \cdot k_{F4} & -0.5\ell \cdot k_{F5} & 0.5\ell \cdot k_{F6} \\ -k_{M1} & k_{M2} & -k_{M3} & k_{M4} & -k_{M5} & k_{M6} \end{pmatrix}, \tag{2.6}$$

$$\boldsymbol{u}_6 = \sum_{i=1}^{6} \omega_{Mi}^2 \boldsymbol{\varepsilon}_{Mi}. \tag{2.7}$$

For octorotors ($p = 4$),

$$\boldsymbol{S}_{\text{rot8}} = \begin{pmatrix} 0 & -\frac{\sqrt{2}}{2}\ell \cdot k_{F2} & -\ell \cdot k_{F3} & -\frac{\sqrt{2}}{2}\ell \cdot k_{F4} & 0 & \frac{\sqrt{2}}{2}\ell \cdot k_{F6} & \ell \cdot k_{F7} & \frac{\sqrt{2}}{2}\ell \cdot k_{F8} \\ \ell \cdot k_{F1} & \frac{\sqrt{2}}{2}\ell \cdot k_{F2} & 0 & -\frac{\sqrt{2}}{2}\ell \cdot k_{F4} & -\ell \cdot k_{F5} & -\frac{\sqrt{2}}{2}\ell \cdot k_{F6} & 0 & \frac{\sqrt{2}}{2}\ell \cdot k_{F8} \\ -k_{M1} & k_{M2} & -k_{M3} & k_{M4} & -k_{M5} & k_{M6} & -k_{M7} & k_{M8} \end{pmatrix}, \tag{2.8}$$

$$\boldsymbol{u}_8 = \sum_{i=1}^{8} \omega_{Mi}^2 \boldsymbol{\varepsilon}_{Mi}. \tag{2.9}$$

For multirotors ($p = 2, 3, 4$),

$$\boldsymbol{S}_{\text{tra}2p} = \begin{pmatrix} 0 & 0 & \cdots & 0 \\ 0 & 0 & \cdots & 0 \\ k_{F1} & k_{F2} & \cdots & k_{F2p} \end{pmatrix}, \tag{2.10}$$

$$\boldsymbol{u}_{2p} = \textstyle\sum_{i=1}^{2p} \omega_{Mi}^2 \boldsymbol{\varepsilon}_{Mi} \tag{2.11}$$

where$span\{\boldsymbol{\varepsilon}_{M1}, \boldsymbol{\varepsilon}_{M2}, \ldots, \boldsymbol{\varepsilon}_{M2p}\}$ arethe basis vectors of a right-handed$2p$-dimensional real vector space$\mathbb{R}^{2p}$.

State equations, maneuver, and flight states (or flight operating points) of multirotors:-

In this subsection, based on the preceding mathematical foundation and [12], dynamical system state equations for a hexarotor are described for clarifying relationships between state variables. Here we show Theorem 1in an explicit form with the Euler angle state variables of dynamical system equations for multirotor rotations.

Theorem 1 [12]:

$$\text{If} \quad \det(\boldsymbol{B}\hat{\boldsymbol{I}}\boldsymbol{B}^{\mathrm{T}}\boldsymbol{\omega}_{\dot{\boldsymbol{x}}}) = -I_{11}I_{22}I_{33}\cos\theta \neq 0, \tag{2.12}$$

the dynamical system state equations for multirotor rotations are written in an explicit form in terms of Euler angle state variables $(\boldsymbol{x}, \dot{\boldsymbol{x}})^{\mathrm{T}} \in \sum_{\text{rot}} \in \mathbb{R}^6$, and the input vector function of time $\boldsymbol{u} \in \Lambda \subset \mathbb{R}^{\rho}$ controls the outer generalized forces acting on the multirotor, then

$$\frac{d}{dt}\begin{pmatrix} \boldsymbol{x} \\ \dot{\boldsymbol{x}} \end{pmatrix} = \begin{pmatrix} \dot{\boldsymbol{x}} \\ \boldsymbol{Y}(\boldsymbol{\eta}, \dot{\boldsymbol{x}}) + \boldsymbol{Z}(\boldsymbol{\eta})\boldsymbol{F}_{\text{rot}}(\boldsymbol{u}) \end{pmatrix}, \tag{2.13}$$

$$\boldsymbol{Z}(\boldsymbol{\eta}) = (\boldsymbol{B}(\boldsymbol{x})\hat{\boldsymbol{I}}\boldsymbol{B}(\boldsymbol{x})^{\mathrm{T}} \cdot \boldsymbol{\omega}_{\dot{\boldsymbol{x}}}(\psi, \theta))^{-1} \cdot \boldsymbol{B}(\boldsymbol{x}), \tag{2.14}$$

$$\boldsymbol{Y}(\boldsymbol{\eta}, \dot{\boldsymbol{x}}) = -(\boldsymbol{B}(\boldsymbol{x})\hat{\boldsymbol{I}}\boldsymbol{B}(\boldsymbol{x})^{\mathrm{T}} \cdot \boldsymbol{\omega}_{\dot{\boldsymbol{x}}}(\psi, \theta))^{-1}(\dot{\boldsymbol{B}}(\boldsymbol{x}, \dot{\boldsymbol{x}})\hat{\boldsymbol{I}}\boldsymbol{B}(\boldsymbol{x})^{\mathrm{T}} \cdot \boldsymbol{\omega}_{\dot{\boldsymbol{x}}}(\psi, \theta) + \boldsymbol{B}(\boldsymbol{x})\hat{\boldsymbol{I}}\boldsymbol{B}(\boldsymbol{x})^{\mathrm{T}} \cdot \dot{\boldsymbol{\omega}}_{\dot{\boldsymbol{x}}}(\psi, \theta, \dot{\psi}, \dot{\theta})) \cdot \dot{\boldsymbol{x}}, \tag{2.15}$$

where $t \in \mathbb{R}$ refers to time, $\boldsymbol{x} = (\psi, \theta, \phi)^{\mathrm{T}} = (\psi, \boldsymbol{\eta})^{\mathrm{T}}, \boldsymbol{\eta} = (\theta, \phi)^{\mathrm{T}}, \dot{\boldsymbol{x}} = (\dot{\psi}, \dot{\theta}, \dot{\phi})^{\mathrm{T}} = \left(\dot{\psi}, \dot{\boldsymbol{\eta}}\right)^{\mathrm{T}}, \dot{\boldsymbol{\eta}} = (\dot{\theta}, \dot{\phi})^{\mathrm{T}}, \boldsymbol{\omega} = \boldsymbol{\omega}_{\dot{\boldsymbol{x}}}\dot{\boldsymbol{x}}$, and $\rho \in \mathbb{N}$.

On the basis of the above equations, we also describe Theorem 2 as an explicit form of dynamical system equations of translation for the multirotor as follows.

Theorem 2 [12]: Let $\left(\boldsymbol{x}(t), \dot{\boldsymbol{x}}(t)\right)^{\mathrm{T}}$ be the solution for Eq. (2.13) in Theorem 1. Then the dynamical system state equation of translation for the multirotor is obtained in the following explicit form:

(2.16) $$\frac{d}{dt}\begin{pmatrix} \boldsymbol{r} \\ \dot{\boldsymbol{r}} \end{pmatrix} = \begin{pmatrix} \dot{\boldsymbol{r}} \\ -g\boldsymbol{e}_3 + \frac{1}{m}\boldsymbol{B}(\boldsymbol{\phi}_1(t, (\boldsymbol{x}_0, \dot{\boldsymbol{x}}_0)^{\mathrm{T}}, \boldsymbol{u}))\boldsymbol{F}_{\mathrm{tra}}(\boldsymbol{u}) \end{pmatrix},$$

where $\left(\boldsymbol{x}(t), \dot{\boldsymbol{x}}(t)\right)^{\mathrm{T}} = (\boldsymbol{\phi}_1(t, (\boldsymbol{x}_0, \dot{\boldsymbol{x}}_0)^{\mathrm{T}}, \boldsymbol{u}), \boldsymbol{\phi}_2(t, (\boldsymbol{x}_0, \dot{\boldsymbol{x}}_0)^{\mathrm{T}}, \boldsymbol{u}))^{\mathrm{T}} = \boldsymbol{\phi}(t, (\boldsymbol{x}_0, \dot{\boldsymbol{x}}_0)^{\mathrm{T}}, \boldsymbol{u}) \in \sum_{\mathrm{rot}} \subset \mathbb{R}^6$ with initial points$(t_0, (\boldsymbol{x}_0, \dot{\boldsymbol{x}}_0)^{\mathrm{T}}) \in \mathbb{R} \times \sum_{\mathrm{rot}} \subset \mathbb{R} \times \mathbb{R}^6$ and $\boldsymbol{u} \in \Lambda$.

We now summarize the dynamical system state equations of the multirotorthe symmetrical standard configurations ($p = 2, 3, 4$), as follows:

(2.17) $$\frac{d}{dt}\begin{pmatrix} \boldsymbol{x} \\ \dot{\boldsymbol{x}} \end{pmatrix} = \begin{pmatrix} \dot{\boldsymbol{x}} \\ \boldsymbol{Y}(\boldsymbol{\eta}, \dot{\boldsymbol{x}}) + \boldsymbol{Z}(\boldsymbol{\eta})\boldsymbol{S}_{\mathrm{rot}2p}\boldsymbol{u}_{2p} \end{pmatrix},$$

(2.18) $$\frac{d}{dt}\begin{pmatrix} \boldsymbol{r} \\ \dot{\boldsymbol{r}} \end{pmatrix} = \begin{pmatrix} \dot{\boldsymbol{r}} \\ -g\boldsymbol{e}_3 + \frac{1}{m}\boldsymbol{B}(\boldsymbol{\phi}_1(t, (\boldsymbol{x}_0, \dot{\boldsymbol{x}}_0)^{\mathrm{T}}, \boldsymbol{u}))\boldsymbol{S}_{\mathrm{tra}2p}\boldsymbol{u}_{2p} \end{pmatrix},$$

Here, by using the state variables of rotational motion $\boldsymbol{x} = (\psi, \theta, \phi)^{\mathrm{T}}, \dot{\boldsymbol{x}} = \left(\dot{\psi}, \dot{\theta}, \dot{\phi}\right)^{\mathrm{T}}$ and translational motion $\boldsymbol{r} = (r_1, r_2, r_3)^{\mathrm{T}}, \dot{\boldsymbol{r}} = (\dot{r}_1, \dot{r}_2, \dot{r}_3)^{\mathrm{T}}$ (Fig. 5), we represent the multirotor maneuver and flight states in many applications as shown in Table 2. The multirotor uses $2p$ fixed motors for flight. The angular velocities of the motors$\boldsymbol{u}_{2p}$are directly used to achieve the flight states in Table 2. In the case that the motion of yaw ψ, pitch θ, and roll $\phi$is fixed, from Eq. (2.17),$d/dt(\boldsymbol{x}, \dot{\boldsymbol{x}})^{\mathrm{T}} = (\boldsymbol{0}_3, \boldsymbol{0}_3)^{\mathrm{T}}$ and $\boldsymbol{0}_3 = (0, 0, 0)^{\mathrm{T}}$hold. Then, as shown in Eq. (2.18), since $\ddot{\boldsymbol{r}}$ depends on $\boldsymbol{x}(t) = \boldsymbol{\phi}_1(t, (\boldsymbol{x}_0, \dot{\boldsymbol{x}}_0)^{\mathrm{T}}, \boldsymbol{u})$,the motion of $r_i$is given by$d/dt\dot{r}_i = \langle \boldsymbol{e}_i, 1/m\, \boldsymbol{B}(\boldsymbol{x})\boldsymbol{S}_{\mathrm{tra}2p}\boldsymbol{u}_{2p}\rangle, i = 1,2$. The motion of r_3 such that multirotors always maintain or control their altitudes is given by$d/dt\dot{r}_3 = \langle \boldsymbol{e}_3, -g\boldsymbol{e}_3 + 1/m\, \boldsymbol{B}(\boldsymbol{x})\boldsymbol{S}_{\mathrm{tra}2p}\boldsymbol{u}_{2p}\rangle$.

Maneuver	Related state variables	Flight state
(i-1) Altitude up control	$r_3$direction, $d/dt\dot{r}_3 > 0$	Lifting the multirotor under gravity and moving it up.
(i-2) Altitude down control	$r_3$direction, $d/dt\dot{r}_3 < 0$	Lifting the multirotor under gravity and moving it down.
(ii) Hover control	r_3 direction, $\dot{r}_1 = \dot{r}_2 = \dot{r}_3 = 0, d/dt\dot{r}_1 = d/dt\dot{r}_2 = d/dt\, \dot{r}_3 = 0, \dot{\psi} = \dot{\theta} = \dot{\phi} = 0$	Being in equilibrium by lifting it under gravity, no rotational motion, and remaining in one place in the air.
(iii-1) Yaw-changing forward control	$\psi, 0 \le \psi < 2\pi, \dot{\psi} > 0$	Yaw changingby counterclockwise turning.
(iii-2) Yaw-changing backward control	$\psi, 0 \le \psi < 2\pi, \dot{\psi} < 0$	Yaw changingby clockwise turning.
(iv-1) Pitch-changing forward control	r_1 direction, $d/dt\dot{r}_1 > 0$, $\theta, 0 \le \theta < \pi/2, \dot{\theta} > 0$	Pitch turning counterclockwise, nose dropping down, tail lifting up, and beginning to accelerate forward.
(iv-2) Pitch-changing backward control	r_1 direction, $d/dt\dot{r}_1 < 0$, $\theta, -\pi/2 < \theta \le 0, \dot{\theta} < 0$	Pitch turning clockwise, nose lifting up, tail dropping down, and beginning to accelerate backward.
(v-1) Roll-changing	r_2 direction, $d/dt\dot{r}_2 > 0$,	Roll turning clockwise, right side lifting

forward control	$\phi, -\pi/2 < \phi \leq 0, \dot{\phi} < 0$	up, left side dropping down, and beginning to accelerate sideways to the left.
(v-2) Roll-changing backward control	r_2 direction, $d/dt\dot{r}_2 < 0$, $\phi, 0 \leq \phi < \pi/2, \dot{\phi} > 0$	Roll turning counterclockwise, right side dropping down, left side lifting up, and beginning to accelerate sideways to the right.

Table 2:- Multirotor maneuver and flight states of Fig. 5 [12].

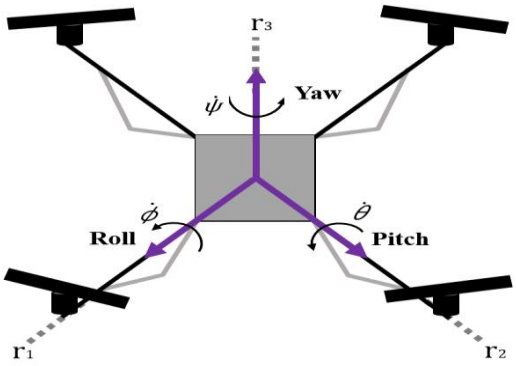

Fig. 5:- Rotational motion and translational motion of the quadrotor (one of the multirotors) [12].

Operating points and equilibrium points of multirotors can be related to the flight states in Table 2. In the following, we describe Definition 1 for the operating points and equilibrium points of multirotors.

*Definition 1 [12]:*Operating points (hereinafter, referred to "flight operating points") of multirotors$(\boldsymbol{x}_{\mathrm{op}}, \dot{\boldsymbol{x}}_{\mathrm{op}})^{\mathrm{T}} \in \mathbb{R}^3 \times \mathbb{R}^3, \boldsymbol{x}_{\mathrm{op}} = (\psi_{\mathrm{op}}, \boldsymbol{\eta}_{\mathrm{op}})^{\mathrm{T}}, \boldsymbol{\eta}_{\mathrm{op}} = (\theta_{\mathrm{op}}, \phi_{\mathrm{op}})^{\mathrm{T}}$, and$(\boldsymbol{r}_{\mathrm{op}}, \dot{\boldsymbol{r}}_{\mathrm{op}})^{\mathrm{T}} \in \mathbb{R}^3 \times \mathbb{R}^3$ are determined as

(2.19) $$\begin{pmatrix} \dot{\boldsymbol{x}}_{\mathrm{op}} \\ \boldsymbol{Z}(\boldsymbol{\eta}_{\mathrm{op}})\boldsymbol{S}_{\mathrm{rot}2p}\boldsymbol{u}_{2p(\mathrm{op})} \end{pmatrix} = \begin{pmatrix} \boldsymbol{0}_3 \\ \boldsymbol{0}_3 \end{pmatrix},$$

(2.20) $$\begin{pmatrix} \dot{r}_{3(\mathrm{op})} \\ \langle \boldsymbol{e}_3, -g\boldsymbol{e}_3 + \frac{1}{m}\boldsymbol{B}(\boldsymbol{x}_{\mathrm{op}})\boldsymbol{S}_{\mathrm{tra}2p}\boldsymbol{u}_{2p(\mathrm{op})} \rangle \end{pmatrix} = \begin{pmatrix} 0 \\ c \end{pmatrix},$$

(2.21) $$\boldsymbol{Z}(\boldsymbol{\eta}_{\mathrm{op}}) = (\boldsymbol{B}(\boldsymbol{x}_{\mathrm{op}})\hat{\boldsymbol{I}}\boldsymbol{B}(\boldsymbol{x}_{\mathrm{op}})^{\mathrm{T}} \cdot \boldsymbol{\omega}_{\dot{\boldsymbol{x}}}(\psi_{\mathrm{op}}, \theta_{\mathrm{op}}))^{-1} \cdot \boldsymbol{B}(\boldsymbol{x}_{\mathrm{op}}),$$

(2.22) $$\ddot{r}_1 = \langle \boldsymbol{e}_1, \frac{1}{m}\boldsymbol{B}(\boldsymbol{x}_{\mathrm{op}})\boldsymbol{S}_{\mathrm{tra}2p}\boldsymbol{u}_{2p(\mathrm{op})} \rangle,$$

(2.23) $$\ddot{r}_2 = \langle \boldsymbol{e}_2, \frac{1}{m}\boldsymbol{B}(\boldsymbol{x}_{\mathrm{op}})\boldsymbol{S}_{\mathrm{tra}2p}\boldsymbol{u}_{2p(\mathrm{op})} \rangle,$$

(2.24) $$\ddot{r}_3 = c,$$

where $c \in \mathbb{R}$is a constant and $\boldsymbol{0}_3 = (0,0,0)^{\mathrm{T}}$. If $c = 0$, the flight operating points $(\boldsymbol{x}_{\mathrm{op}}, \dot{\boldsymbol{x}}_{\mathrm{op}})^{\mathrm{T}}$ and $(\boldsymbol{r}_{\mathrm{op}}, \dot{\boldsymbol{r}}_{\mathrm{op}})^{\mathrm{T}}$have a constant altitude. Further, if $\dot{r}_1 = \dot{r}_2 = \ddot{r}_1 = \ddot{r}_2 = 0$ and $c = 0$ (i.e., $\ddot{r}_3 = 0$), the flight operating points are also identified as equilibrium points $(\boldsymbol{x}_{\mathrm{e}}, \dot{\boldsymbol{x}}_{\mathrm{e}})^{\mathrm{T}}$ and$(\boldsymbol{r}_{\mathrm{e}}, \dot{\boldsymbol{r}}_{\mathrm{e}})^{\mathrm{T}}$ and occur in hovering flight.

Problem of multirotor stable flights to avoid a crash:-

In this section, in the case of complete propeller motor failures, we describe a method of providing motor speed control signals to achieve flight states to avoid a crash [12]. We assume that the motors in the i_1th, i_2th, …, i_nth rotors $(1 \leq i_1 < i_2 < \cdots < i_n \leq 2p, 1 \leq n \leq 2p-2, p = 2,3,4, n \in \mathbb{N})$ have completely failed. Then the motor speed control signal vector of the remaining motors is determined by

(3.1) $$\boldsymbol{u}_{2p-n}^{i_1,i_2,\ldots,i_n} = \sum_{j=1}^{i_1-1} \omega_{Mj}^2 \boldsymbol{\varepsilon}_{Mj} + \sum_{j=i_1+1}^{i_2-1} \omega_{Mj}^2 \boldsymbol{\varepsilon}_{Mj} + \cdots + \sum_{j=i_n+1}^{2p} \omega_{Mj}^2 \boldsymbol{\varepsilon}_{Mj}.$$

The remaining moments of $\boldsymbol{S}_{\mathrm{rot}2p}\boldsymbol{u}_{2p-n}^{i_1,i_2,\ldots,i_n}$ and the remaining translational forces of $\boldsymbol{S}_{\mathrm{tra}2p}\boldsymbol{u}_{2p-n}^{i_1,i_2,\ldots,i_n}$, $p = 2, 3, 4$, are respectively given as

$$\boldsymbol{S}_{\mathrm{rot}2p}\boldsymbol{u}_{2p-n}^{i_1,i_2,\ldots,i_n} = \boldsymbol{S}_{\mathrm{rot}2p-n}^{i_1,i_2,\ldots,i_n}\boldsymbol{u}_{2p-n}^{i_1,i_2,\ldots,i_n}, \tag{3.2}$$

$$\boldsymbol{S}_{\mathrm{tra}2p}\boldsymbol{u}_{2p-n}^{i_1,i_2,\ldots,i_n} = \boldsymbol{S}_{\mathrm{tra}2p-n}^{i_1,i_2,\ldots,i_n}\boldsymbol{u}_{2p-n}^{i_1,i_2,\ldots,i_n}, \tag{3.3}$$

where $\boldsymbol{S}_{\xi 2p-n}^{i_1,i_2,\ldots,i_n}$ is the matrix $\boldsymbol{S}_{\xi 2p}$ with the i_1th, i_2th, …, i_nth rows deleted ($\xi = \mathrm{rot}, \mathrm{tra}$).

Here,we summarize the state equations of the multirotors with the symmetrical standard configurations ($p = 2, 3, 4$)in the case of complete propeller motor failures using the Euler angle rotational equation [Eq. (2.17)]and the translational equation [Eq. (2.18)] as follows:

$$\frac{d}{dt}\begin{pmatrix} \boldsymbol{x} \\ \dot{\boldsymbol{x}} \end{pmatrix} = \begin{pmatrix} \dot{\boldsymbol{x}} \\ \boldsymbol{Y}(\boldsymbol{\eta}, \dot{\boldsymbol{x}}) + \boldsymbol{Z}(\boldsymbol{\eta})\boldsymbol{S}_{\mathrm{rot}2p-n}^{i_1,i_2,\ldots,i_n}\boldsymbol{u}_{2p-n}^{i_1,i_2,\ldots,i_n} \end{pmatrix}, \tag{3.4}$$

$$\frac{d}{dt}\begin{pmatrix} \boldsymbol{r} \\ \dot{\boldsymbol{r}} \end{pmatrix} = \begin{pmatrix} \dot{\boldsymbol{r}} \\ -g\boldsymbol{e}_3 + \frac{1}{m}\boldsymbol{B}(\boldsymbol{x})\boldsymbol{S}_{\mathrm{tra}2p-n}^{i_1,i_2,\ldots,i_n}\boldsymbol{u}_{2p-n}^{i_1,i_2,\ldots,i_n} \end{pmatrix}. \tag{3.5}$$

In [12] in the case of complete propeller motor failures, theflight operating points and equilibrium points of multirotorsare related to the two types of multirotor flight states in Table 3 to avoid a crash when some motors fail and stop. for the flight operating points and equilibrium points of multirotors to achieve the flight states in Table 3 to avoid a crashwhen some motors fail and stop, Definition 2 is given. Based on Definition 2, a methodto provide motor speed control signals to achieve the flight states in Table 3to avoid a crash is proposed and verified by several simulations. However, in this paper, we only consider the case of Type (I) in Table 3. We provide theorems of the stabilizability of the flight states for avoiding a crash and stabilizing such flight states by nonlinear dynamic state equations with state variable feedbacks. We alsoverify the therems by simulations.

Type	Achieved flight states in Table 2
(I) No Problem	All (e.g., in Fig. 6).
(II) Admissible Problem	Yaw angles cannot be controlled. Yaw angles are freely changing (e.g., in Fig. 7).

Table 3:- Two types of multirotor flight states to avoid a crash [12].

Type (I): Among the remaining motors, some must be stopped to achieve all states in Table 2 when certain motors fail and stop.
Type (II): Among the remaining motors, some must be stopped to achieve all states (except for yaw control) in Table 2 when certain motors fail and stop.
Type (I) and type (II) represent the severity levels of complete propeller motor failure. Type (I) and type (II) are determined by the equation forms of Eq. (41) in Method 1. Type (II) is more severe than type (I) because yaw angles cannot be controlled.

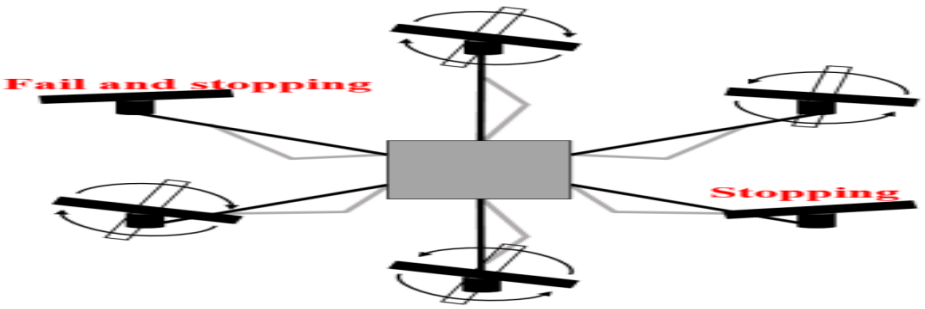

Fig. 6:- Example of type (I)no problemwhere one of the remaining motors must be stopped to achieve all the states of the hexarotor in Table 2 when one motor fails and stops [12].

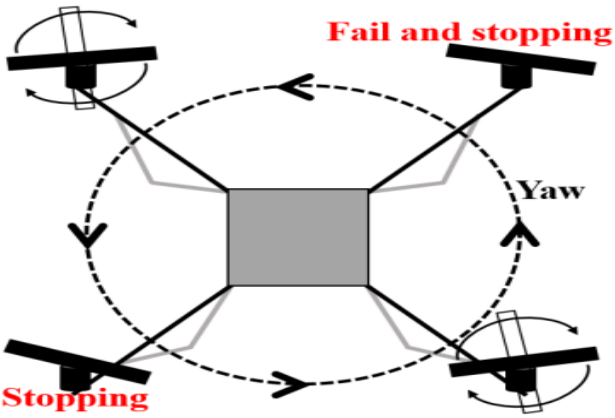

Fig. 7:- Example of type (II) admissible problem where one of the remaining motors must be stopped to achieve all states(except for yaw control)of the quadrotor in Table 2 when one motor fails and stops [12].

Definition 2 [12]: When some motors fail and stop, the flight operating points of multirotors to achieve the flight states in the case of Type (I) in Table 3 $(\boldsymbol{x}_{\mathrm{op}}, \dot{\boldsymbol{x}}_{\mathrm{op}})^{\mathrm{T}} \in \mathbb{R}^3 \times \mathbb{R}^3, \boldsymbol{x}_{\mathrm{op}} = (\psi_{\mathrm{op}}, \boldsymbol{\eta}_{\mathrm{op}})^{\mathrm{T}}, \boldsymbol{\eta}_{\mathrm{op}} = (\theta_{\mathrm{op}}, \phi_{\mathrm{op}})^{\mathrm{T}}$, and$(\boldsymbol{r}_{\mathrm{op}}, \dot{\boldsymbol{r}}_{\mathrm{op}})^{\mathrm{T}} \in \mathbb{R}^3 \times \mathbb{R}^3$to avoid a crash are determined as

$$\begin{pmatrix} \dot{\boldsymbol{x}}_{\mathrm{op}} \\ \boldsymbol{Z}(\boldsymbol{\eta}_{\mathrm{op}})\boldsymbol{S}_{\mathrm{rot}2p-n}^{i_1,i_2,\ldots,i_n}\boldsymbol{u}_{2p-n(\mathrm{op})}^{i_1,i_2,\ldots,i_n} \end{pmatrix} = \begin{pmatrix} \boldsymbol{0}_3 \\ \boldsymbol{0}_3 \end{pmatrix}, \tag{3.6}$$

$$\begin{pmatrix} \dot{r}_{3(\mathrm{op})} \\ \langle \boldsymbol{e}_3, -g\boldsymbol{e}_3 + \frac{1}{m}\boldsymbol{B}(\boldsymbol{x}_{\mathrm{op}})\boldsymbol{S}_{\mathrm{tra}2p-n}^{i_1,i_2,\ldots,i_n}\boldsymbol{u}_{2p-n(\mathrm{op})}^{i_1,i_2,\ldots,i_n} \rangle \end{pmatrix} = \begin{pmatrix} 0 \\ c \end{pmatrix}, \tag{3.7}$$

$$\boldsymbol{Z}(\boldsymbol{\eta}_{\mathrm{op}}) = (\boldsymbol{B}(\boldsymbol{x}_{\mathrm{op}})\hat{\boldsymbol{I}}\boldsymbol{B}(\boldsymbol{x}_{\mathrm{op}})^{\mathrm{T}} \cdot \boldsymbol{\omega}_{\dot{\boldsymbol{x}}}(\psi_{\mathrm{op}}, \theta_{\mathrm{op}}))^{-1} \cdot \boldsymbol{B}(\boldsymbol{x}_{\mathrm{op}}), \tag{3.8}$$

$$\ddot{r}_1 = \langle \boldsymbol{e}_1, \frac{1}{m}\boldsymbol{B}(\boldsymbol{x}_{\mathrm{op}})\boldsymbol{S}_{\mathrm{tra}2p-n}^{i_1,i_2,\ldots,i_n}\boldsymbol{u}_{2p-n(\mathrm{op})}^{i_1,i_2,\ldots,i_n} \rangle, \tag{3.9}$$

$$\ddot{r}_2 = \langle \boldsymbol{e}_2, \frac{1}{m}\boldsymbol{B}(\boldsymbol{x}_{\mathrm{op}})\boldsymbol{S}_{\mathrm{tra}2p-n}^{i_1,i_2,\ldots,i_n}\boldsymbol{u}_{2p-n(\mathrm{op})}^{i_1,i_2,\ldots,i_n} \rangle, \tag{3.10}$$

$$\ddot{r}_3 = c, \tag{3.11}$$

where $c \in \mathbb{R}$is a constant and $\boldsymbol{0}_3 = (0,0,0)^{\mathrm{T}}$. If $c = 0$, the flight operating points $(\boldsymbol{x}_{\mathrm{op}}, \dot{\boldsymbol{x}}_{\mathrm{op}})^{\mathrm{T}}$ and $(\boldsymbol{r}_{\mathrm{op}}, \dot{\boldsymbol{r}}_{\mathrm{op}})^{\mathrm{T}}$have a constant altitude. Further, if $\dot{r}_1 = \dot{r}_2 = \ddot{r}_1 = \ddot{r}_2 = 0$ and $c = 0$ (i.e., $\ddot{r}_3 = 0$), the flight operating points are called equilibrium points $(\boldsymbol{x}_{\mathrm{e}}, \dot{\boldsymbol{x}}_{\mathrm{e}})^{\mathrm{T}}$ and$(\boldsymbol{r}_{\mathrm{e}}, \dot{\boldsymbol{r}}_{\mathrm{e}})^{\mathrm{T}}$ and occur in hovering flights.

Further, we provide Theorem 3 based on Definition 2 to provide motor speed control signals to achieve the flight states in the case of Type (I) in Table 3.

Theorem 3: For the hexarotorcase of complete propeller motor failures,let $\boldsymbol{F}\left(\boldsymbol{x}, \boldsymbol{u}_{6-n}^{i_1,\ldots,i_n}\right)$ be the following C^1 function taking values in $\mathbb{R}^{6-n}$ with a neighborhood of Euler angle state variables $\tilde{\boldsymbol{x}}$ in $\mathbb{R}^3$ and the motor speed control signal vector of the remaining motors$\tilde{\boldsymbol{u}}_{6-n}^{i_1,\ldots,i_n} \in \mathbb{R}^{6-n}$, with $\boldsymbol{F}\left(\tilde{\boldsymbol{x}}, \tilde{\boldsymbol{u}}_{6-n}^{i_1,\ldots,i_n}\right) = \boldsymbol{0}_{6-n} = (0,\ldots,0)^{\mathrm{T}}$,including both lower sections of $\boldsymbol{Z}(\boldsymbol{\eta}_{\mathrm{o}})\boldsymbol{S}_{rot-n}^{i_1,\ldots,i_n}\boldsymbol{u}_{6-n(op)}^{i_1,\ldots,i_n}$ in Eq. (3.6) and $\langle \boldsymbol{e}_3, -g\boldsymbol{e}_3 + \frac{1}{m}\boldsymbol{B}(\boldsymbol{x}_{\mathrm{o}})\boldsymbol{S}_{tra-n}^{i_1,\ldots,i_n}\boldsymbol{u}_{6-n(op)}^{i_1,\ldots,i_n} \rangle$ in Eq. (3.7):

$$\boldsymbol{F}\left(\boldsymbol{x}, \boldsymbol{u}_{6-n}^{i_1,\ldots,i_n}\right) = \boldsymbol{A}_{6-n}^{i_1,\ldots,i_n}(\boldsymbol{x})\boldsymbol{u}_{6-n}^{i_1,\ldots,i_n} - \boldsymbol{b}_{6-n}, \tag{3.12}$$

$$\boldsymbol{A}_{6-n}^{i_1,\ldots,i_n}(\boldsymbol{x}) \in \mathbb{R}^{(6-n)\times(6-n)} = \begin{pmatrix} \boldsymbol{A'}_{4\times(6-n)}^{i_1,\ldots,i_n}(\boldsymbol{\eta}) \\ \boldsymbol{Q}_{2\times(6-n)} \end{pmatrix}, \tag{3.13}$$

$$\boldsymbol{A'}_{4\times(6-n)}(\boldsymbol{\eta}) \in \mathbb{R}^{4\times(6-n)} = \begin{pmatrix} \boldsymbol{Z}(\boldsymbol{\eta})\boldsymbol{S}_{rot6-n}^{i_1,\ldots,i_n} \\ \boldsymbol{e}_3^{\mathrm{T}}\frac{1}{m}\boldsymbol{B}(\boldsymbol{x})\boldsymbol{S}_{tra6-n}^{i_1,\ldots,i_n} \end{pmatrix}, \tag{3.14}$$

$$\boldsymbol{b}_{6-n} = (\ddot{\psi}, \ddot{\theta}, \ddot{\phi}, c + g, \boldsymbol{b}_2)^{\mathrm{T}}, \quad (3.15)$$

where $c \in \mathbb{R}$ is a constant and $\boldsymbol{Q}_{2\times(6-n)} \in \mathbb{R}^{2\times(6-n)}$is a constant matrix. $\boldsymbol{b}_{6-n} \in \mathbb{R}^{6-n}$ and $\boldsymbol{b}_2 \in \mathbb{R}^2$ is a constant vector.If for arbitrary $\tilde{\boldsymbol{x}} \in \mathbb{R}^3$, $(i)\det(\boldsymbol{A}_{6-n}^{i_1,\ldots,i_n}(\tilde{\boldsymbol{x}})) \neq 0$, and (ii) there exists$\tilde{\boldsymbol{u}}_{6-n}^{i_1,\ldots,i_n} \in \mathbb{R}^{6-n}$such that $\boldsymbol{F}\left(\tilde{\boldsymbol{x}}, \tilde{\boldsymbol{u}}_{6-n}^{i_1,\ldots,i_n}\right) = \boldsymbol{0}_{6-n}$,then$\tilde{\boldsymbol{u}}_{6-n}^{i_1,\ldots,i_n} = \boldsymbol{A}_{6-n}^{i_1,\ldots,i_n}(\tilde{\boldsymbol{x}})^{-1}\boldsymbol{b}_{6-n}$ is uniquely obtained.
Then $\ddot{\psi}$, $\ddot{\theta}$, and $\ddot{\phi}$ are also determined as

$$\begin{aligned}
\ddot{\psi} &= \langle \boldsymbol{\varepsilon}_1, \boldsymbol{Y}(\boldsymbol{\eta}, \dot{\boldsymbol{x}}) + \boldsymbol{Z}(\boldsymbol{\eta})\boldsymbol{S}_{rot6-n}^{i_1,\ldots,i_n}\boldsymbol{u}_{6-n}^{i_1,\ldots,i_n}\rangle, \\
\ddot{\theta} &= \langle \boldsymbol{\varepsilon}_2, \boldsymbol{Y}(\boldsymbol{\eta}, \dot{\boldsymbol{x}}) + \boldsymbol{Z}(\boldsymbol{\eta})\boldsymbol{S}_{rot6-n}^{i_1,\ldots,i_n}\boldsymbol{u}_{6-n}^{i_1,\ldots,i_n}\rangle, \\
\ddot{\phi} &= \langle \boldsymbol{\varepsilon}_3, \boldsymbol{Y}(\boldsymbol{\eta}, \dot{\boldsymbol{x}}) + \boldsymbol{Z}(\boldsymbol{\eta})\boldsymbol{S}_{rot6-n}^{i_1,\ldots,i_n}\boldsymbol{u}_{6-n}^{i_1,\ldots,i_n}\rangle.
\end{aligned} \quad (3.16)$$

Thus,$\tilde{\boldsymbol{u}}_{6-n}^{i_1,\ldots,i_n} \in \square^{6-n}$are obtained as the motor speed control signals to achieve the flight states in the case of Type (I) in Table 3 to avoid a crash. As the number of failed motors$n$ increases, the rank of$\boldsymbol{S}_{rot6-n}^{i_1,\ldots,i_n} \in \square^{3\times(6-n)}$ or $\boldsymbol{S}_{tra6-n}^{i_1,\ldots,i_n} \in \square^{3\times(6-n)}$ and the dimensionality of$\boldsymbol{u}_{6-n}^{i_1,\ldots,i_n} \in \square^{6-n}$decrease.Therefore, since $\boldsymbol{A}_{6-n}^{i_1,\ldots,i_n} \in \square^{(6-n)\times(6-n)}$ is not a square matrix, it is necessary to remove arbitrary rows to obtain square matrices.
The proof of Theorem 3 is provided in a similar way to that in the proof of either Theorem3 or Theorem4 in [12].

Linearized or nonlinear dynamic state equations to stabilize the flights for avoiding a crash
This subsection describes linearized or nonlinear dynamic state equations to stabilize thehexarotor flights for avoiding a crash the case of type (I)in Table 3.

In the case of type (I) in Table 3 ($1 \leq i_1 < \cdots < i_n \leq 6, 1 \leq n \leq 2, n \in \square$), we obtain the following variational differential equations with constant matrices at the operating points $(\boldsymbol{x}_o, \dot{\boldsymbol{x}}_0)^{\mathrm{T}}$which can be used to stabilize the hexarotor flights in the case of type (I) in Table 3.

$$\frac{d}{dt}\delta\boldsymbol{X}_{rot} = \boldsymbol{F}_{rot6-n(op)}\delta\boldsymbol{X}_{rot} + \boldsymbol{G}_{rot6-n(op)}\delta\boldsymbol{U}_{6-n}^{i_1,\ldots,i_n}, \quad (3.17)$$

$$\delta\boldsymbol{X}_{rot} = (\delta\boldsymbol{x}, \delta\dot{\boldsymbol{x}})^{\mathrm{T}},$$

$$(\delta\boldsymbol{x}, \delta\dot{\boldsymbol{x}})^{\mathrm{T}} = (\boldsymbol{x} - \boldsymbol{x}_{(op)}, \dot{\boldsymbol{x}} - \dot{\boldsymbol{x}}_{(op)})^{\mathrm{T}}, \quad (3.18)$$

$$\boldsymbol{F}_{rot6-n(op)} = \begin{pmatrix} \boldsymbol{0}_{3\times3} & \boldsymbol{I}_{3\times3} \\ f_{rot\boldsymbol{x}}(\boldsymbol{\eta}_{op}, \dot{\boldsymbol{x}}_{op}, \boldsymbol{u}_{6-n(op)}^{i_1,\ldots,i_n}) & f_{rot\dot{\boldsymbol{x}}}(\boldsymbol{\eta}_{op}, \dot{\boldsymbol{x}}_{op}) \end{pmatrix}, \quad (3.19)$$

$$\boldsymbol{G}_{rot6-n(op)} = \begin{pmatrix} \boldsymbol{0}_{3\times(6-n)} \\ f_{rot\boldsymbol{u}_{6-n}^{i_1,\ldots,i_n}}(\boldsymbol{\eta}_{op}) \end{pmatrix}, \quad (3.20)$$

$$f_{rot\boldsymbol{\zeta}}(\boldsymbol{\eta}_{op}, \dot{\boldsymbol{x}}_{op}, \boldsymbol{u}_{6-n(op)}^{i_1,\ldots,i_n}) = \boldsymbol{Y}_{\boldsymbol{\zeta}}(\boldsymbol{\eta}_{op}, \dot{\boldsymbol{x}}_{op}) + \left[\frac{\partial}{\partial\boldsymbol{\zeta}}\left(\boldsymbol{Z}(\boldsymbol{\eta})\boldsymbol{S}_{rot6-n}^{i_1,\ldots,i_n}\boldsymbol{u}_{6-n(op)}^{i_1,\ldots,i_n}\right)\right|_{\boldsymbol{\eta}=\boldsymbol{\eta}_{op}}, \quad (3.21)$$

$$f_{rot\dot{\boldsymbol{\zeta}}}(\boldsymbol{\eta}_{op}, \dot{\boldsymbol{x}}_{op}) = \boldsymbol{Y}_{\dot{\boldsymbol{\zeta}}}(\boldsymbol{\eta}_{op}, \dot{\boldsymbol{x}}_{op}), \quad (3.22)$$

$$f_{rot\boldsymbol{u}_{6-n}^{i_1,\ldots,i_n}}(\boldsymbol{\eta}_{op}) = \boldsymbol{Z}(\boldsymbol{\eta}_{op})\boldsymbol{S}_{rot6-n}^{i_1,\ldots,i_n}, \quad (3.23)$$

where $\boldsymbol{\zeta} = \boldsymbol{x} \in \square^3$, or $\boldsymbol{\eta} \in \square^2$, $\dot{\boldsymbol{\zeta}} = \dot{\boldsymbol{x}} \in \square^3$, or $\dot{\boldsymbol{\eta}} \in \square^2$, $\boldsymbol{0}_{3\times(6-n)}$ is the $3 \times (6-n)$ zero matrix.
$\boldsymbol{Y}_{\boldsymbol{x}}$ and $\boldsymbol{Y}_{\dot{\boldsymbol{x}}}$ denotes the partial derivative of $\boldsymbol{Y}$ with respect to $\boldsymbol{x}$ and $\boldsymbol{Y}$ with respect to $\dot{\boldsymbol{x}}$, respectively.
$f_{rot\boldsymbol{x}}$, $f_{rot\dot{\boldsymbol{x}}}$, and $f_{rot\boldsymbol{u}_{6-n}^{i_1,\ldots,i_n}}$ denotes the partial derivative of $f_{rot}$with respect to $\boldsymbol{x}$, f_{rot} with respect to $\dot{\boldsymbol{x}}$, and $\square_{\square\square\square}$ with respect to$\square_{6-\square}^{\square_1,\ldots,\square_{\square}}$respectively.

*Theorem 4:*In thehexarotor case of type (I) in Table 3 ($1 \leq \square_1 < \cdots < \square_{\square} \leq 6$, $1 \leq \square \leq 2$, and $\square \in \square$), let $\square_{\square rot-\square(op)} \in \square^{6\times(6\times(6-\square))}$ be a $6 \times \left(6 \times (6-\square)\right)$, controllability matrix defined as Eq. (3.24).

$$C_{Mrot6-n(op)} = [G_{rot6-n(op)}, F_{rot6-n(op)}G_{rot6-n(op)}, F^{2}_{rot6-n(op)}G_{rot6-n(op)}, \ldots, F^{5}_{rot6-n(op)}G_{rot6-n(op)}], \quad (3.24)$$

If $\square_{\square\square\square\square 6-\square(\square\square)}$ has full rank 6, namely the constant matrix pair $(\square_{\square\square\square 6-\square(\square\square)}, \square_{\square\square\square 6-\square(\square\square)})$ is completely controllable, there exists a $(6-\square)\times 6$ constant matrix $\square_{6-\square(\square\square)}$ such that every solution of Eq. (3.25) approaches the origin vector of Eq. (3.25) $\square_6 = (0,\ldots,0)^{\mathrm{T}} \in \square^6$ (i.e., the origin is asymptotically stable), and that the variational acceleration $\square\ddot{\square}$ approaches the origin vector $\square_3 = (0,0,0)^{\mathrm{T}} \in \square^3$, by Eq. (3.26).

$$\frac{d}{dt}\delta \boldsymbol{X}_{\mathrm{rot}} = (\boldsymbol{F}_{\mathrm{rot}6-n(\mathrm{op})} - \boldsymbol{G}_{\mathrm{rot}6-n(\mathrm{op})}\boldsymbol{K}_{6-n(\mathrm{op})})\delta \boldsymbol{X}_{\mathrm{rot}}, \quad (3.25)$$

$$\delta \ddot{\boldsymbol{r}} = \frac{1}{m}\left[\frac{\partial}{\partial \boldsymbol{x}}\left(\boldsymbol{B}(\boldsymbol{x})\boldsymbol{S}^{i_1,\ldots,i_n}_{\mathrm{tra}6-n}\boldsymbol{u}^{i_1,\ldots,i_n}_{6-n(\mathrm{op})}\right)\right]\Bigg|_{\boldsymbol{x}=\boldsymbol{x}_{\mathrm{op}}}\delta \boldsymbol{x} - \frac{1}{m}\boldsymbol{B}(\boldsymbol{x}_{\mathrm{op}})\boldsymbol{S}^{i_1,\ldots,i_n}_{\mathrm{tra}6-n}\boldsymbol{K}_{6-n(\mathrm{op})}\delta \boldsymbol{X}_{\mathrm{rot}}, \quad (3.26)$$

where $\square\square_{\square\square\square} = (\square\square, \square\dot{\square})^{\mathrm{T}}$ and $\square\dot{\square} = \dot{\square} - \dot{\square}_{\square\square}$.

Proof: In the hexarotorcase of type (I) in Table 3 ($1 \le \square_1 < \cdots < \square_\square \le 6$, $1 \le \square \le 2$, $\square \in \square$), for arbitrary constant matrix $\square_{6-\square(\square\square)} \in \square^{(6-\square)\times 6}$, substituting $\square\square^{\square_1,\ldots,\square_\square}_{6-\square} = -\square_{6-\square(\square\square)}\square\square_{\square\square\square}$ into Eq. (3.17), the closed-loop system equations of Eq. (3.25) is obtained. Since $\square_{\square\square\square\square 6-\square(\square\square)}$ has full rank 6, namely the matrix pair $(\square_{\square\square\square 6-\square(\square\square)}, \square_{\square\square\square 6-\square(\square\square)})$is completely controllable, it is proved that there exists a constant matrix $\square_{6-\square(\square\square)}$ such that all eigenvalues of $\square_{\square\square\square 6-\square(\square\square)} - \square_{\square\square\square 6-\square(\square\square)}\square_{6-\square(\square\square)}$ have negative real parts from [21]. In the case that all eigenvalues of $\square_{\square\square\square 6-\square(\square\square)} - \square_{\square\square\square 6-\square(\square\square)}\square_{6-\square(\square\square)}$ have negative real parts, every solution of Eq. (3.25) approaches the origin vector $\square_6$, and by Eq. (3.26) $\square\square_{\square\square\square} \to \square_6$, (then $\square\square \to \square_3$) implies $\square\ddot{\square} \to \square_3$.

Theorem 5: In the hexarotorcase of type (I) in Table 3 ($1 \le \square_1 < \cdots < \square_\square \le 6$, $1 \le \square \le 2$, and $\square \in \square$), $(\square)$ if $\square_{\square\square\square\square 6-\square(\square\square)}$ of Eq. (3.24) has full rank 6, then substituting $\square\square^{\square_1,\ldots,\square_\square}_{6-\square} = \square\square\square^{\square_1,\ldots,\square_\square}_{6-\square} = -\square_{6-\square(\square\square)}(\square - \square_{(\square\square)}, \dot{\square} - \dot{\square}_{(\square\square)})^{\mathrm{T}}$, into the dynamical system state equations of Eq. (3.4) and Eq. (3.5), the following closed-loop equations of Eq. (3.27) and Eq. (3.30) are obtained.Further $(\square\square)$ if all eigenvalues of Jacobian matrix $(\square_{\square\square\square 6-\square(\square\square)} - \square_{\square\square\square 6-\square(\square\square)}\square_{6-\square(\square\square)})$ have negative real parts, then the solutions of Eq. (3.27): $(\square(t, (\square_0, \dot{\square}_0)^{\mathrm{T}}), \dot{\square}(t, (\square_0, \dot{\square}_0)^{\mathrm{T}}))$ with initial points $(\square_0, (\square_0, \dot{\square}_0)^{\mathrm{T}})$ near $(\square_{\square\square}, \dot{\square}_{\square\square})^{\mathrm{T}}$, approach to $(\square_{\square\square}, \dot{\square}_{\square\square})^{\mathrm{T}}$, and by Eq. (3.30), the acceleration $\ddot{\square}(\square)$ approaches the operating point vector $\ddot{\square}_{(\square\square)}$.

$$\frac{d}{dt}\begin{pmatrix} \boldsymbol{x} \\ \dot{\boldsymbol{x}} \end{pmatrix} = \begin{pmatrix} \dot{\boldsymbol{x}} \\ f_{rot}(\boldsymbol{x}, \dot{\boldsymbol{x}}) \end{pmatrix}, \quad (3.27)$$

$$\boldsymbol{M} = \begin{pmatrix} \boldsymbol{0}_{3\times 3} & \boldsymbol{I}_{3\times 3} \end{pmatrix}, \quad (3.28)$$

$$f_{rot}(\boldsymbol{x}, \dot{\boldsymbol{x}}) = \boldsymbol{Y}(\boldsymbol{\eta}, \dot{\boldsymbol{x}}) + \boldsymbol{Z}(\boldsymbol{\eta})\boldsymbol{S}^{i_1,\ldots,i_n}_{rot6-n}(\boldsymbol{u}^{i_1,\ldots,i_n}_{6-n(op)} + \delta \boldsymbol{u}^{i_1,\ldots,i_n}_{6-n}), \quad (3.29)$$

$$\frac{d}{dt}\begin{pmatrix} \boldsymbol{r} \\ \dot{\boldsymbol{r}} \end{pmatrix} = \begin{pmatrix} \dot{\boldsymbol{r}} \\ f_{tra}(\boldsymbol{\varphi}(t, (\boldsymbol{x}_0, \dot{\boldsymbol{x}}_0)^{\mathrm{T}}), \dot{\boldsymbol{\varphi}}(t, (\boldsymbol{x}_0, \dot{\boldsymbol{x}}_0)^{\mathrm{T}})) \end{pmatrix}, \quad (3.30)$$

$$f_{tra}(\boldsymbol{x}, \dot{\boldsymbol{x}}) = -g\boldsymbol{e}_3 + \frac{1}{m}\boldsymbol{B}(\boldsymbol{x})\boldsymbol{S}^{i_1,\ldots,i_n}_{tra6-n}(\boldsymbol{u}^{i_1,\ldots,i_n}_{6-n(op)} + \delta \boldsymbol{u}^{i_1,\ldots,i_n}_{6-n}), \quad (3.31)$$

where $\square_{6-\square(\square\square)}$: a constant matrix defined in Theorem 4, $(\square\square, \square\dot{\square})^{\mathrm{T}} = (\square - \square_{(\square\square)}, \dot{\square} - \dot{\square}_{(\square\square)})^{\mathrm{T}}$, $(\square(\square), \dot{\square}(\square))^{\mathrm{T}} = (\square(t, (\square_0, \dot{\square}_0)^{\mathrm{T}}), \dot{\square}(t, (\square_0, \dot{\square}_0)^{\mathrm{T}}))^{\mathrm{T}} = (\square(t, (\square_0, \dot{\square}_0)^{\mathrm{T}}, \square^{\square_1,\ldots,\square_\square}_{6-\square(\square\square)} + \square\square^{\square_1,\ldots,\square_\square}_{6-\square}), \dot{\square}(t, (\square_0, \dot{\square}_0)^{\mathrm{T}}, \square^{\square_1,\ldots,\square_\square}_{6-\square(\square\square)} + \square\square^{\square_1,\ldots,\square_\square}_{6-\square}))^{\mathrm{T}} \in \Sigma_{\square\square\square} \subset \square^6$ with initial points $(\square_0, (\square_0, \dot{\square}_0)^{\mathrm{T}}) \in \square \times \square$ and $\square^{\square_1,\ldots,\square_\square}_{6-\square(\square\square)} + \square\square^{\square_1,\ldots,\square_\square}_{6-\square} \in \Lambda$, and $\square$: a neighborhood of $(\square_{\square\square}, \dot{\square}_{\square\square})^{\mathrm{T}}$ in $\Sigma_{\square\square\square} \subset \square^6$ such that $\|(\square_0 - \square_{\square\square}, \dot{\square}_0 - \dot{\square}_{\square\square})^{\mathrm{T}}\| < 1$.

Proof: In the hexarotorcase of type (I) in Table 3 ($1 \le \square_1 < \cdots < \square_\square \le 6$, $1 \le \square \le 2$, $\square \in \square$), we utilize Hartman-Grobman theorem in [9], and for arbitrary constant matrix $\square_{6-\square(\square\square)} \in \square^{(6-\square)\times 6}$, substituting $\delta\square^{\square_1,\ldots,\square_\square}_{6-\square}(\square, \dot{\square}) = -\square_{6-\square(\square\square)}(\square - \square_{(\square\square)}, \dot{\square} - \dot{\square}_{(\square\square)})^{\mathrm{T}}$, into the dynamical system state equations of Eq. (3.4) and

Eq. (3.5), the following closed-loop equations of Eq. (3.27) and Eq. (3.30) are obtained. Since $\square_{\square\square\square\square 6-\square(\square\square)}$ of Eq. (3.24) has full rank *6*, there exists a constant matrix $\square_{6-\square(\square\square)}$ such that all eigenvalues of $\square_{\square\square\square\square 6-\square(\square\square)}$ - $\square_{\square\square\square\square 6-\square(\square\square)}\square_{6-\square(\square\square)}$of Eq. (3.27) have negative real parts from Theorem 4. Further since all eigenvalues of Jacobian matrix ($\square_{\square\square\square\square 6-\square(\square\square)}$- $\square_{\square\square\square\square 6-\square(\square\square)}\square_{6-\square(\square\square)}$) have negative real parts, it is proved that the solutions of Eq. (3.27): ($\square(t, (\square_0, \dot{\square}_0)^T)$, $\dot{\square}(t, (\square_0,\dot{\square}_0)^T)$) with initial points ($\square_0$, $(\square_0,\dot{\square}_0)^T)\in \square \times \square$ near $(\square_{\square\square},\dot{\square}_{\square\square})^T$ and the linearized flow map ($\square\square(t, (\square_{\square\square},\dot{\square}_{\square\square})^T)$, $\square\dot{\square}(t, (\square_{\square\square},\dot{\square}_{\square\square})^T)$) ($\square_0$ - $\square_{(\square\square)}$, $\dot{\square}_0$- $\dot{\square}_{(\square\square)}$)^T are topologically equivalent from the Hartman-Grobman theorem. Namely, since the linearized flow map is asymptotically stable, ($\square(t, (\square_0, \dot{\square}_0)^T)$, $\dot{\square}(t, (\square_0,\dot{\square}_0)^T)$) with initial points ($\square_0$, $(\square_0,\dot{\square}_0)^T)\in \square \times \square$ near $(\square_{\square\square},\dot{\square}_{\square\square})^T$ is also asymptotically stable. Thus by Eq. (3.30), theacceleration$\ddot{\square}(\square)$ approaches the operating point vector$\ddot{\square}_{(\square\square)}$.

Simulations of the hexarotor stable flights to avoid a crash:-

In this section, we present typical examples of Type (I) of the hexarotor stable flight states in Table 3 to avoid a crash in the case of complete propeller motor failures. We verify Theorem 3–5 of realizing the hexarotor stable flights to achieve the flight states in the case of Type (I) in Table 3 to avoid a crash. The following results are obtained by using Theorem 3–5 with Maple symbolic computations, MATLAB matrix calculations, and MATLAB numerical simulations with the ode45 solver [10].Notice that regarding the translational state equation of the hexarotor [Eq. (3.5)] the numerical computations in the following figures are carried out using the computation results obtained from the Euler angles state equation of the hexarotor [Eq. (3.4)] together with piecewise linear interpolations [17] of $\square(\square)$, $\square(\square)$, and $\square(\square)$.

The numerical parameters of a hexarotor, are given in Table 4.

Symbol	Description	Value and unit
m	Total mass of the hexarotor	2 (kg)
I_{11}	Moment of inertia of the hexarotor	0.02973 (kg ·m^2)
I_{22}	Moment of inertia of the hexarotor	0.02931 (kg ·m^2)
I_{33}	Moment of inertia of the hexarotor	0.048315 (kg ·m^2)
g	Gravitational acceleration	9.80665 (m/s^2)
k_F	Motor force coefficients of the hexarotor	1.79×10^{-7} (N/rpm^2)
k_M	Motor moment coefficients of the hexarotor	4.38×10^{-9}(Nm/rpm^2)
ℓ	Distance from each rotor to geometric center of the hexarotor	0.365 (m)

Table 4:- Numerical parameters of a hexarotor ($p = 3$) [12].

In addition, we define the constant matrix of $\square_{(2\square-4)\times 2\square} \in \square^{(2\square-4)\times 2\square}$, $\square = 3$, as follows:
the hexarotor ($\square = 3$),

(4.1)
$$\boldsymbol{Q}_{2\times 6} = \begin{pmatrix} 0 & 1 & -1 & 0 & 0 & 0 \\ 0 & 0 & 0 & 1 & -1 & 0 \end{pmatrix},$$

where $\square_{(2\square-4)\times 2\square}$in Eq. (3.13) in Theorem 3.

In the following, we assume that under complete propeller motor failures, the hexarotor is in a hover control: maneuver (ii) in Table 2, as well as possible.As an example of type(I) in Table 3, we also assume the motor failure case such that the motor in the first rotor has completely failed (in Fig. 8), as follows.

Flight state: $\square_{(\square\square)} = \square_{(\square\square)} = \square_{(\square\square)} = 0$[rad], $\dot{\square}_{(\square\square)} = \dot{\square}_{(\square\square)} = \dot{\square}_{(\square\square)} = 0$ [rad/s^2], $\square_{1(\square\square)} = \square_{2(\square\square)} = 0$ [m], $\square_{3(\square\square)} = 3$ [m], $\dot{\square}_{1(\square\square)} = \dot{\square}_{2(\square\square)} = \dot{\square}_{3(\square\square)} = 0$ [m/s], c (or$\ddot{\square}_3$) = 0 [m/s^2], Motor control signal vector (Motor rotating speed): $\omega_{\square 2(\square\square)} = \omega_{\square 3(\square\square)} = \omega_{\square 5(\square\square)} = \omega_{\square 6(\square\square)} = 5233.8205$ [rpm],$\omega_{\square 4(\square\square)} = 0$ [rpm].

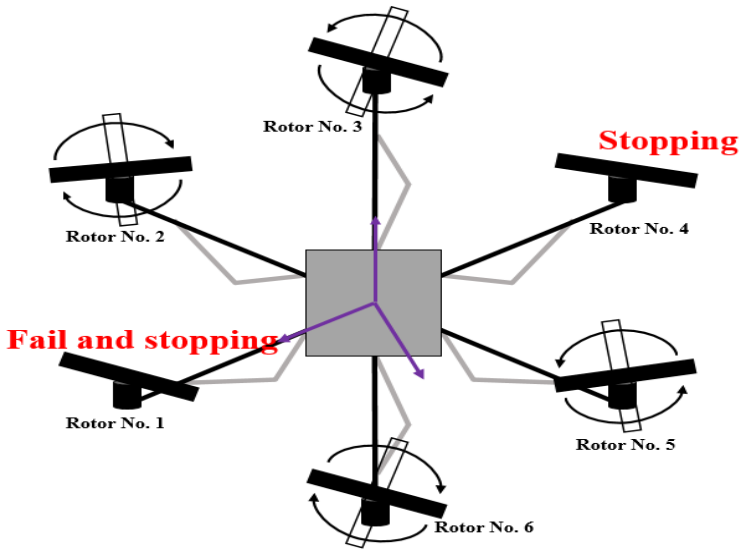

Fig. 8:- An example of type(I) in Table 3: the motor in the first rotor has completely failed

Theorem 3 is applied to the example of (a):-
(a) Under the condition (t [s] ∈ [*0 1*]) in the case of Fig. 8, we ascertained the following flight simulation result of the flight state to avoid a crash (type (I) in Table 3, maneuver (ii) in Table 2) as shown in Fig. 9 and Fig. 10. □(□), □(□), and □(□) in Fig. 9 completely overlap. □$_1$(□) and □$_2$(□) in Fig. 10 also completely overlap.

In this case, the function □(□, □$^{□_1,\ldots,□_□}_{6-□}$) in Theorem 3 is as follows:

$$\boldsymbol{F}(\boldsymbol{\eta}, \boldsymbol{u}_5^{i_1}) = \boldsymbol{A}_5^{i_1}(\boldsymbol{\eta})\boldsymbol{u}_5^{i_1} - \boldsymbol{b}_5, \tag{4.2}$$

$$\boldsymbol{A}_5^{i_1}(\boldsymbol{\eta}) \in \mathbb{R}^{5\times5} = \begin{pmatrix} \boldsymbol{A'}_{4\times5}(\boldsymbol{\eta}) \\ \boldsymbol{\varepsilon}_{Qk}^{\mathrm{T}} \boldsymbol{Q}_{2\times5}^{i_1} \end{pmatrix}, \tag{4.3}$$

$$\boldsymbol{A'}_{4\times5}(\boldsymbol{\eta}) \in \mathbb{R}^{4\times5} = \begin{pmatrix} \boldsymbol{Z}(\boldsymbol{\eta})\boldsymbol{S}_{rot5}^{i_1} \\ \boldsymbol{e}_3^{\mathrm{T}} \frac{1}{m}\boldsymbol{B}(\boldsymbol{x})\boldsymbol{S}_{tra5}^{i_1} \end{pmatrix}, \tag{4.4}$$

$$\boldsymbol{b}_5 = (\ddot{\psi}, \ddot{\theta}, \ddot{\phi}, c + g, \boldsymbol{b}_1)^{\mathrm{T}} \in \mathbb{R}^5, \tag{4.5}$$

where □$_1$ = *1*, k = 1, □$^{□_1}_{2\times5}$ ∈ □$^{2\times5}$, and □$_1$ ∈ □.*span*{□$_{□1}$, □$_{□2}$} are the basis vectors of a right-handed two-dimensional real vector space □^{2}.□$^{□_1}_{2\times5}$ is the matrix □$_{2\times6}$ with the□$_1$th (or 1th) row deleted. □$^{□_1}_{ξ5}$ is the matrix □$_{ξ6}$ with the □$_1$th (or 1th) row deleted (ξ = rot, tra).

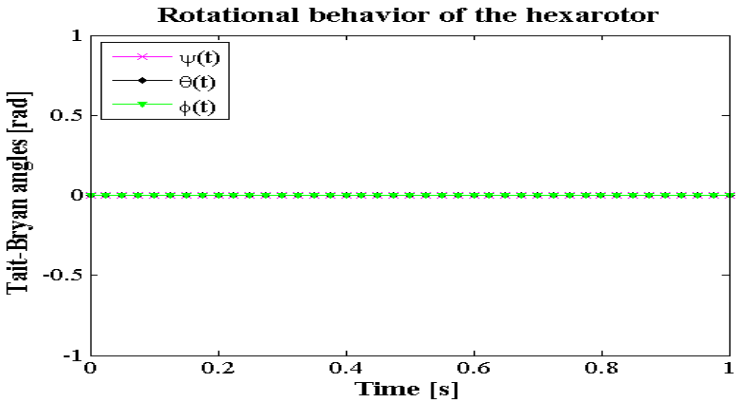

Fig. 9:- Simulation results of Tait-Bryan angles when the motor of the first rotor has completely failed (example (a)).

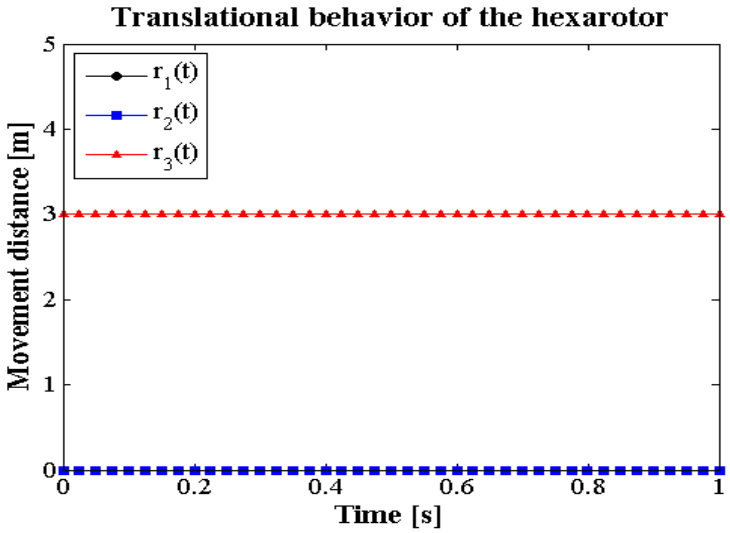

Fig. 10:- Simulation results for position of motion when the motor of the first rotors has completely failed ($□_3 = 3$ [m]: initial condition) (example (a)).

The example of (a) verifies that Theorem 3 achieves the hexarotor flight states to avoid a crashe (type (I) in Table 3) using the remaining motors of the hexarotor in the case of complete propeller motor failure, even without any feedbacks.

Theorem 4 is applied to the examples of (b).

(b) Under the following conditions in the case of Fig. 8: as an application of Theorem 4, as follows.
For the hexarotor when the motor of the first rotor has completely failed, we choose the constant matrix $□_{5(□□)} ∈ □^{5×6}$ as follws:

$$\boldsymbol{K}_{5(op)} \in \mathbb{R}^{5\times 6} = 10^{11}\cdot\begin{pmatrix} 0.8273 & -0.0336 & -0.0591 & 0.0083 & -0.0003 & -0.0006 \\ -0.8273 & 0.0336 & -0.0591 & -0.0083 & 0.0003 & -0.0006 \\ 1.6546 & 0.1346 & 0 & 0.0165 & 0.0013 & 0 \\ -0.8273 & 0.0336 & 0.0591 & -0.0083 & 0.0003 & 0.0006 \\ 0.8273 & -0.0336 & 0.0591 & 0.0083 & -0.0003 & 0.0006 \end{pmatrix}. \quad (4.6)$$

Then the eigenvalues of $□_{□□□5(□□)} - □_{□□□5(□□)}□_{5(□□)}$ of Eq. (3.25) are -300, -300, -300, -150, -150, and -150, respectively. Thus, the closed-loop system of Eq. (3.25) is asymptotically stable.

The simulation initial values are set as follows (t [s] $∈ [0\ 0.1]$):
1. $□□(0) = 0.00174533$ [rad], $□□(0) = 0$ [rad], $□□(0) = 0$ [rad], $□\dot{□}(0) = 0$ [rad/s], $δ\dot{□}(0) = 0$ [rad/s], and $□\dot{□}(0) = 0$[rad/s].
2. $□_{□□} = 0$ [rad], $□_{□□} = 0$ [rad], $\dot{□}_{□□} = 0$ [rad/s], $\dot{□}_{□□} = 0$ [rad/s], $\dot{□}_{op} = 0$ [rad/s], $□_{□2(□□)} = □_{□3(□□)} = □_{□5(□□)} = □_{□6(□□)} = 5233.8205$[rpm], and $□_{□4(□□)} = 0$[rpm].

Typical behavior of the closed-loop system of Eq. (3.25) is illustrated in Fig.11 and Fig.12, typical behavior of the variational acceleration $δ\ddot{□}$ of Eq. (3.26) is illustrated in Fig.13 and Fig.14, and the remaining motor speed control signals of state variable feedback controls are illustrated in Fig.15.
$δθ(□)$ and $δϕ(□)$in Fig. 11 completely overlap and
$□/□□δθ(□)$and $□/□□δϕ(□)$ in Fig. 12 also completely overlap.
$δ□_1(□)$ and $δ□_2(□)$ in Fig.13 completely overlap and
$□/□□\ δ□_1(□)$ and $□/□□\ δ□_2(□)$ in Fig.14 also completely overlap.
$δ□_2(□)$ and $δ□_6(□)$,$δ□_3(□)$ and $δ□_5(□)$ in Fig.15 completely overlap.

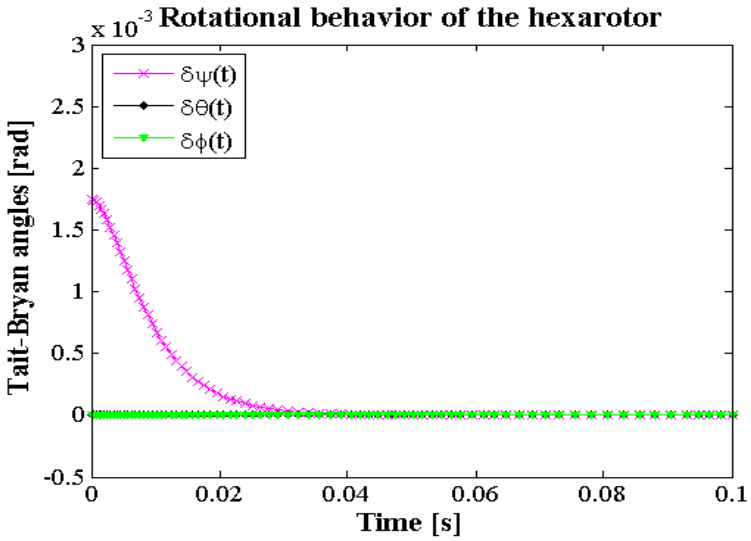

Fig. 11:- Simulation results of Tait-Bryan angles for stabilizing a flight for avoiding a crash with state variable feedbacks by linearized state equations, when the motor of the first rotor has completely failed (example (b)).

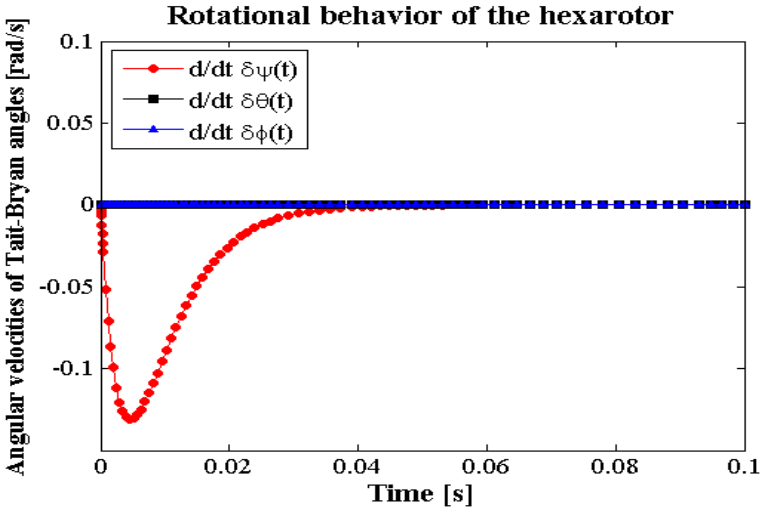

Fig. 12:- Simulation results of angular velocities of Tait-Bryan angles for stabilizing a flight for avoiding a crash with state variable feedbacks by linearized state equations, when the motor of the first rotor has completely failed (example (b)).

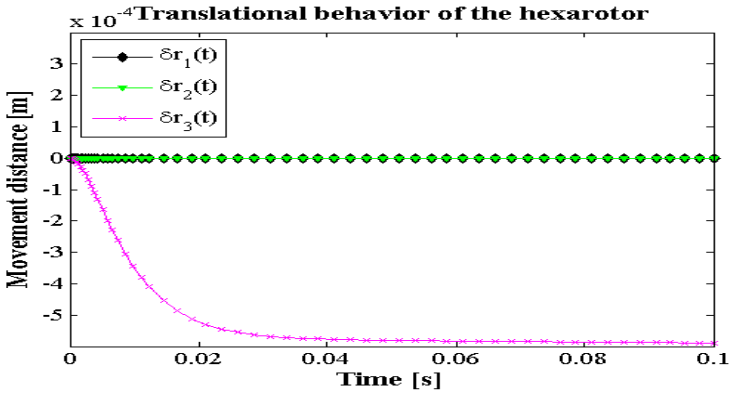

Fig. 13:- Simulation results for position of motion for stabilizing a flight for avoiding a crash with state variable feedbacks by linearized state equations, when the motor of the first rotors has completely failed (example (b)).

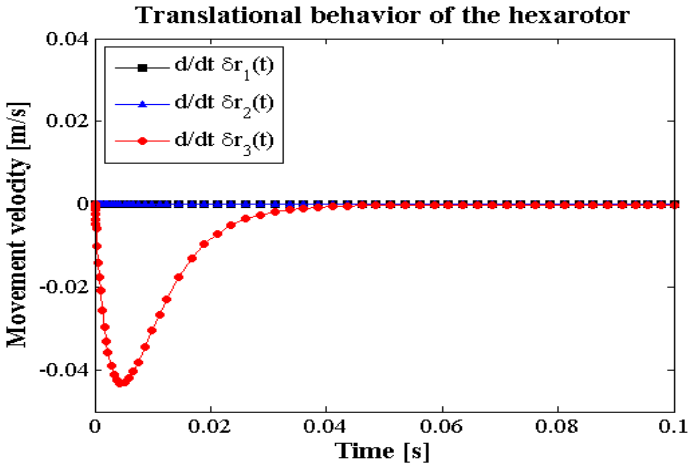

Fig. 14:- Simulation results for velocities of motion for stabilizing a flight for avoiding a crash with state variable feedbacks by linearized state equations, when the motor of the first rotors has completely failed (example (b)).

This example of (b) verifies that Theorem 4 stabilizes the hexarotor flight states to avoid a crash (type (I) in Table 3) using the remaining motors of the hexarotor in the case of complete propeller motor failure.

Theorem 5 is applied to the example of (c) with $\square_{5(\square\square)}$in Eq. (4.6).

(c) Under the following conditions in the case of Fig. 8 as an application of Theorem 5, as follows.
The simulation initial values are set as follows (t[s]∈ [*0 0.1*]):
1. $\square\square(0) = 0.00174533$ [rad], $\square\square(0) = 0$ [rad], $\square\square(0) = 0$ [rad], $\square\dot{\square}(0) = 0$ [rad/s], $\delta\dot{\square}(0) = 0$ [rad/s], and $\square\dot{\square}(0) = 0$[rad/s].
2. $\square_{\square\square} = 0$ [rad], $\square_{\square\square} = 0$ [rad], $\dot{\square}_{\square\square} = 0$ [rad/s], $\dot{\square}_{\square\square} = 0$ [rad/s], $\dot{\square}_{op} = 0$ [rad/s], $\square_{\square 2(\square\square)} = \square_{\square 3(\square\square)} = \square_{\square 5(\square\square)} = \square_{\square 6(\square\square)} = 5233.8205$[rpm], and$\square_{\square 4(\square\square)} = 0$[rpm].

Typical behavior of the Euler angles state equation with state variable feedbacks of Eq. (3.27) is illustrated in Fig.15 and Fig.16, typical behavior of the translational state equation with state variable feedbacks of Eq. (3.30) is illustrated in Fig.17 and Fig.18, and the remaining motor speed control signals for realizing a stable flight for avoiding a crash with state variable feedbacks by nonlinear state equations, are illustrated in Fig.19.

$\square\square(\square)$ and$\square\square(\square)$in Fig.15 completely overlap and
$\square/\square\square\square\square(\square)$and $\square/\square\square\square\square(\square)$ in Fig.16 also completely overlap.
$\square\square_1(\square)$ and$\square\square_2(\square)$ in Fig.17 completely overlap and
$\square/\square\square\ \square\square_1(\square)$ and $\square/\square\square\ \square\square_2(\square)$ in Fig.18 also completely overlap.
$\delta\square_2(\square)$ and $\square\square_6(\square)$,$\square\square_3(\square)$ and $\square\square_5(\square)$ in Fig.19 completely overlap.

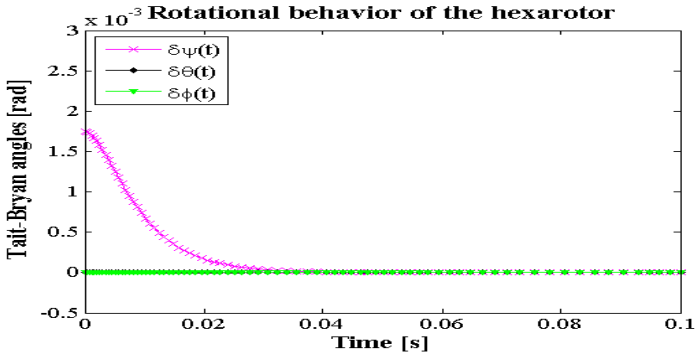

Fig. 15:- Simulation results of Tait-Bryan angles for realizing a stable flight for avoiding a crash with state variable feedbacks by nonlinear state equations, when the motor of the first rotor has completely failed (example (c)).

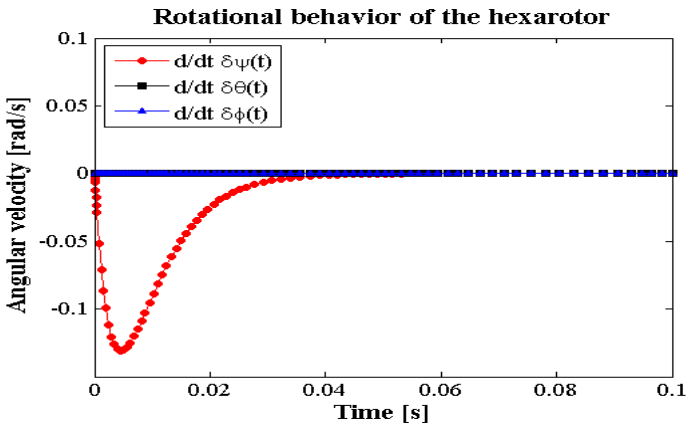

Fig. 16:- Simulation results of angular velocities of Tait-Bryan angles for realizing a stable flight for avoiding a crash with state variable feedbacks by nonlinear state equations, when the motor of the first rotor has completely failed (example (c)).

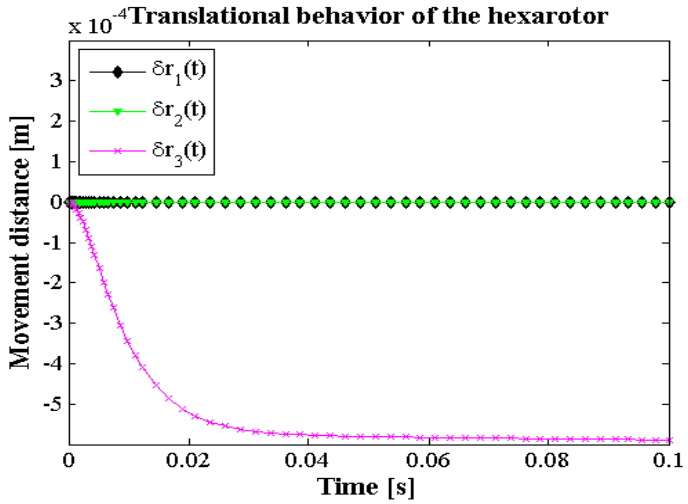

Fig. 17:- Simulation results for position of motion for realizing a stable flight for avoiding a crash with state variable feedbacks by nonlinear state equations, when the motor of the first rotors has completely failed (example (c)).

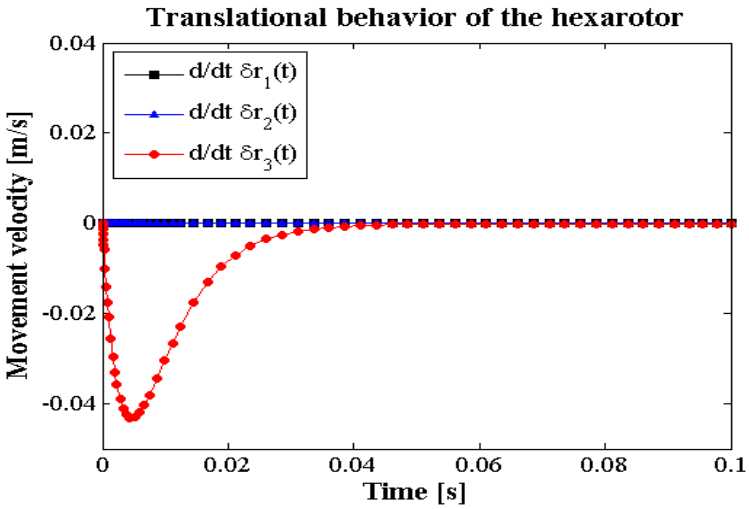

Fig. 18:- Simulation results for velocities of motion for realizing a stable flight for avoiding a crash with state variable feedbacks by nonlinear state equations, when the motor of the first rotors has completely failed (example (c)).

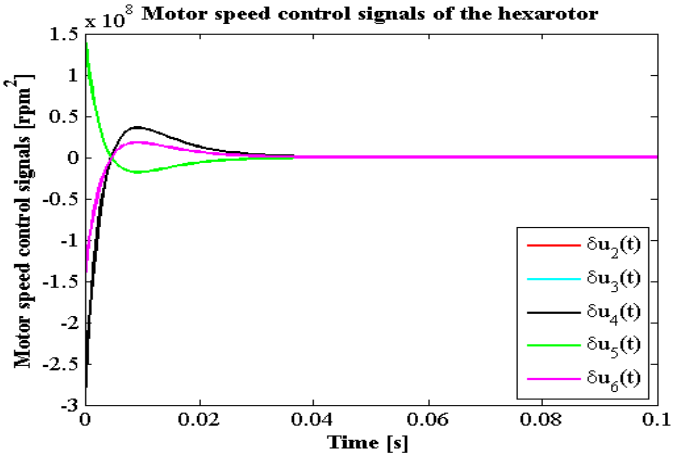

Fig. 19:- Simulation results for the remaining motor control signals for realizing a stable flight for avoiding a crash with state variable feedbacks by nonlinear state equations, when the motor of the first rotors has completely failed (example (c)).

This example of (c) verifies that Theorem 5 achieves the hexarotor stable flight states to avoid a crash (type (I) in Table 3) using the remaining motors of the hexarotor in the case of complete propeller motor failure.

Conclusion:-

The following results were obtained:

1. We have provided Theorem 3 based on Definition 2 to provide motor speed control signals to achieve the flight states in the case of Type (I) in Table 3.
2. We have provided Theorem 4 of stabilizability of the operating points for the hexarotor flights to avoid a crash in the case of Type (I) in Table 3, and Theorem 5 of nonlinear hexarotor dynamic state equations with state variable feedbacks to stabilize flight states to avoid a crash in the case of Type (I) in Table 3.
3. We have presented typical example of Type(I) of hexarotor stable flight states in Table 3 to avoid a crash, and verified Theorem 3–5.
4. we will build a state variable feedback control for stabilizing themultirotor flight statesin the case of Type (II) in Table 3 under the influence of disturbances such as wind.
5. We will verify theorems experimentally through several tests of actual multirotor flights to avoid a crash in the case of complete propeller failures using a commercial multirotor model with modifications based ontheorems.

References:-

1. Arnold V. I. (1997): Mathematical Methods of Classical Mechanics, Second Edition. Springer-Verlag.
2. Dongjie S., Binxian Y., and Quan Q. (2016): ``Reliability Analysis of Multicopter Configurations Based on Controllability Theory," Proceedings of the 35th Chinese Control Conference July 27-29 Chengdu, China, pp. 6740–6745.
3. Eriksson E., Estep D., and Johnson C. (2004): Applied Mathematics: Body and Soul, vol. 2, pp. 621–626, Springer Verlag.
4. Falcon′i G. P., Marvakov V. A. and Holzapfel F. (2016): ``Fault Tolerant Control for a Hexarotor System using Incremental Backstepping," 2016 IEEE Conference on Control Applications (CCA) Part of 2016 IEEE Multi-Conference on Systems and Control, pp. 237–242, 19-22, 2016. Buenos Aires, Argentina.
5. Freddi A., Lanzon A., and Longhi S. (2011): ``A feedback linearization approach to fault tolerance in quadrotor vehicles," 18th IFAC World Congress, pp. 5413–5418, Milano Italy August 28 – September 2.
6. Giribet J. I., Peña R. S. S., and Ghersin A. S. (2016): ``Analysis and design of a tilted rotor hexacopter for fault tolerance," IEEE Transactions on aerospace and electronic systems 52.4 (2016): 1555-1567.
7. Giribet J. I. et al (2018): ``Experimental validation of a fault-tolerant hexacopter with tilted rotors," IngenieríaElectrónica [7] (2018). http://ri.itba.edu.ar/handle/123456789/1557
8. Goldstein H. (1980): CLASSICAL MECHANICS, 2nd Edn. Addison-Wesley.
9. Guckenheimer J. and Holmes P. (1983): Nonlinear Oscillations, Dynamical Systems, and Bifurcations of Vector Fields, Springer-Verlag.
10. Higham D. J. and Higham N. J. (2005): MATLAB Guide, Second Edition, pp. 175–184, SIAM.

11. Isogai K., Nakano H., and Okazaki H. (2018): ``Modeling and Flight Control Simulation of Multirotors," 2018 IEEE 61th International Midwest Symposium on Circuits and Systems (The IEEE MWSCAS 2018), pp. 388–392, 5–8 August 2018, Windsor, Canada.
12. Isogai K., Nakano H., and Okazaki H. (2019): How to Avoid a Multirotor Flight Crash under Complete Propeller Motor Failures Based on State Variable Approach, Sens. Mater., Vol. 31, No. 12, pp. 4173–4203. https://myukk-org.ssl-xserver.jp/SM2017/article.php?ss=2418
13. Moon F. C. (1998): Applied Dynamics: With Applications to Multibody and Mechatronic System, pp. 103–167, pp. 168–253, pp. 474–477, John Wiley and Sons Inc..
14. Mazeh H., Saied M., Shraim H., and Francis C. (2018): ``Fault-Tolerant Control of an Hexarotor Unmanned Aerial Vehicle Applying Outdoor Tests and Experiments," IFAC PapersOnline 51-22 (2018) 312–317.
15. Mueller M. W.andD'Andrea R., (2014): ``Stability and control of a quadrocopter despite the complete loss of one, two, or three propellers," 2014 IEEE International Conference on Robotics Automation (ICRA) Hong Kong Convention and Exhibition Center May 31 – June 7, Hong Kong, China, pp. 45–52.
16. Okazaki H., Isogai K., and Nakano H. (2016): ``Modeling and Simulation of Motion of a Quadcopter in a Light Wind," 2016 IEEE 59th International Midwest Symposium on Circuits and Systems (The IEEE MWSCAS 2016), pp. 117–120, 16–19 October 2016, Abu Dhabi, UAE.
17. Okazaki H., Yashikida K., and Mizutani H. (2012): ``A one dimensional mapping method for time series data," 2012 IEEE 55th International Midwest Symposium, on Circuits and Systems (MWSCAS), pp. 490–493.
18. Okazaki H., Yin S., Isogai K., and Nakano H. (2018): ``Motor speed control signals for multirotor flights in the presence of complete propeller motor failures," 2018 IEEE 61th International Midwest Symposium on Circuits and Systems (The IEEE MWSCAS 2018), pp. 384–387, 5–8 August 2018, Windsor, Canada.
19. Saied M., Lussier B., Fantoni I., Shraim, H. and Francis C. (2017): ``Fault Diagnosis and Fault-Tolerant Control of an Octorotor UAV using motors speeds measurements," IFAC PapersOnline 50-1, 5263–5268.
20. S′anchez Pena R. S., Alonso R., and Anigstein P. (2000): ``Robust optimal solution to the attitude/force control problem," IEEE Transactions on aerospace and electronic systems 36.3: 784–792.
21. Wonham W. M. (1967): ``On Pole Assignment in Multi-Input Controllable Linear Systems," IEEE Transactions on Automatic Control, vol. AC. 12, no. 6, pp. 660–665.
22. Yamamoto Y. (2012): From Vector Spaces to Function Spaces - Introduction to Functional Analysis with Applications -, pp. 203–207, SIAM, 2012.